A Numerical Solution of a Surface Crack under Cyclic Hydraulic Pressure Loading

Z.-Q. Xu[2], K. J. Hsia[1]

Department of Theoretical and Applied Mechanics

University of Illinois at Urbana-Champaign, Urbana, IL 61801, USA

March, 1996

Submitted to: *ASME Journal of Tribology*

[1]Author to whom correspondence should be addressed.

[2]On leave from Shanghai University, Shanghai, China.

ABSTRACT

Material degradation and failure in rolling contact components is often associated with surface crack initiation and propagation under repeated contact loading. In the presence of lubricating fluid, the pressure in the fluid film between the contacting surfaces may play an important role in the crack growth process. This paper presents a method to model the effect of hydraulic pressure loading on surface crack growth. The governing equations of the coupled viscous fluid/ cracked solid problem are obtained, which are non-linear integral and differential equations. The fluid is assumed to be Newtonian and incompressible. The cracked solid is considered to be linear elastic. Pressure loading history is prescribed at the crack mouth. Finite difference method is used to solve the governing equations. For each time step, Newton-Raphson iteration method is used to search the root of the non-linear equations. Both transient and steady state pressure distribution under cyclic pressure loading can be obtained using this method. A few numerical examples are given to demonstrate the reliability and effectiveness of the solution method. The solution shows that there exists a characteristic time which determines whether pressure fluctuations at the crack mouth can be transmitted deep into the crack. The steady state pressure distribution exhibits a phase delay from the applied cyclic loading.

1. Introduction

Deterioration and failure of rolling contact components such as bearings and gears is usually caused by surface pitting and spalling resulting from tiny surface crack propagation under repeated contact loading (Suh, 1986). Since most of these components are lubricated by liquid lubricants, the growth of surface cracks involves interaction between the cracked solid and the lubricating fluid. Therefore, a thorough understanding of crack growth behavior under the influence of lubricating fluid is essential to the understanding of failure of rolling contact components.

One interesting experimental observation of the surface crack growth process is that, in the absence of lubricating fluid, the surface crack grows very slowly; whereas with lubricating fluid, the crack grows much faster (Way, 1935; Kaneta and Murakami, 1987). This phenomenon may be explained by the hydraulic pressure in the fluid during rolling contact loading. Since lubricating oil is viscous fluid, the pressure build-up underneath the roller in the fluid thin film is extremely high, often on the order of a few GPa (Clarke et al, 1985). Whether this high pressure will enhance the surface crack growth depends on whether it can be transmitted deep into the crack. Thus the pressure distribution within the crack for given pressure loading history plays a crucial role in the pressure-induced crack growth process.

The physical process of hydraulic pressure-induced crack growth is schematically shown in Figure 1. As the roller approaches the crack, in addition to the mode II stress intensity caused by the contact loading, the pressure at the crack mouth increases. This increase will cause the crack to open up. However, the opening up of the crack demands the fluid to flow into the crack to fill the enlarged volume within the crack. To achieve this, the pressure gradient in the crack-filling fluid increases. The absolute value of the pressure deep inside the crack may even decrease upon applied loading. The pressure at the crack mouth reaches the peak when the center of the roller passes the crack. As the roller rolls away from the surface crack, the pressure at the mouth decreases. The direction of the pressure gradient within the crack is then reversed. The lubricating fluid is squeezed out gradually due to elastic response of the cracked body. This process is repeated as the roller rolls over the crack periodically such as in a bearing or a gear.

Two major factors affecting this process are: deformation of the cracked solid which is usually elastic; and flow of the viscous fluid within the crack. Fatigue crack growth in the presence of fluid has been studied by many researchers (e.g., Tzou, et al, 1985a, 1985b) and reviewed by Srivat-

san and Sudarshan (1988). However, the effects of hydraulic pressure loading have not been considered in these studies. Hydraulic pressure effect under transient condition was considered by others (Bower, 1988; Kaneta & Murakami, 1987; Michau et al, 1974). But the fully coupled fluid-solid interaction was not accounted for. On the other hand, the fluid-solid interaction problem in rolling contact components has been extensively studied by researchers in the tribology community. And time-dependent behavior of pressure distribution and fluid film thickness profile has recently been studied by several people (Johnson, 1985; Houpert and Hamrock, 1986; Chang et al, 1989a, 1989b; Ai and Zhang, 1989; Osborn and Sadeghi, 1992; Venner and Lubrecht, 1994). However, in the current problem, there exists an additional degree of complication due to stress singularity at the crack tip.

In the present communication, we consider the effects of hydraulic pressure loading alone. The mathematical framework of surface crack propagation under hydraulic pressure loading was laid out by Hsia and Xu (1996). In their paper, by imposing a strong assumption, an approximate analytic solution was obtained by separation of variables. An estimate of a characteristic penetration time was also obtained, which determines whether the pressure fluctuation at the crack mouth can be transmitted deep into the crack. Here a numerical solution of the governing equations is sought. This paper focuses on the numerical techniques to deal with the complicated non-linear governing equations. A few numerical examples will be given to demonstrate the reliability of the solution method.

2. Governing Equations

Although the real problem is very complicated, involving perhaps compressible fluid, non-Newtonian viscous flow in a confined geometry, and curved crack shapes, a much simplified, ideal case is considered in the present study. The fluid is considered to be incompressible and Newtonian. Only a straight crack normal to the specimen surface as shown in Fig. 2 is studied. It is also assumed that there is no leakage of fluid in the crack.

The governing equations of the simplified problem consist of two parts: one for the viscous fluid inside the crack; and one for the cracked solid. The governing equation for the fluid inside the crack, considering the incompressibility condition, can be derived as (Hsia and Xu, 1996)

$$\frac{\partial H}{\partial t} = \frac{1}{12\mu}\frac{\partial}{\partial x}\left(H^3\frac{\partial p}{\partial x}\right), \tag{1}$$

where $H(x, t)$ and $p(x, t)$ are the crack opening displacement and the pressure distribution at location x and time t, respectively (see Fig. 2), and μ is the viscosity of the fluid.

The governing equation for an elastic solid body under a distributed crack face pressure, $p(x, t)$, can be obtained as (Bueckner, 1970),

$$H(x, t) = \int_0^a G(s, x)\, p(s, t)\, ds, \tag{2}$$

where $G(s, x)$ is the Green's function for the contribution of the pressure at s to the crack opening displacement at location x, and a is the crack length as shown in Fig. 2.

For normalization purpose, we introduce a reference time, τ, as

$$\tau = 12\mu/E'. \tag{3}$$

where $E' = E/(1-\nu^2)$ for plane strain and $E' = E$ for plane stress deformation, respectively, with E being the Young's modulus and ν the Poisson's ratio of the solid. The governing equations can then be simplified to non-dimensional forms by introducing the following normalization,

$$\begin{cases} \bar{x} = x/a \\ \bar{t} = t/\tau \\ \bar{H} = H/a \\ \bar{p} = p/E' \\ \bar{G}(\bar{s}, \bar{x}) = G(s, x)\, E' \end{cases}, \tag{4}$$

Equations (1) and (2) then become,

$$\frac{\partial \bar{H}}{\partial \bar{t}} = \frac{\partial}{\partial \bar{x}} \left(\bar{H}^3 \frac{\partial \bar{p}}{\partial \bar{x}} \right) \tag{1a}$$

$$\bar{H}(\bar{x}, \bar{t}) = \int_0^1 \bar{G}(\bar{s}, \bar{x})\, \bar{p}(\bar{s}, \bar{t})\, d\bar{s}. \tag{2a}$$

The detailed derivation of the dimensionless Green's function, $\bar{G}(\bar{s}, \bar{x})$, is given in Appendix A (Tada, et al, 1985). For a surface crack in an infinite elastic body as that shown in Fig. 2, the Green's function is given by

$$\bar{G}(\bar{s}, \bar{x}) = \frac{8}{\pi} \int_{max(\bar{s}, \bar{x})}^{1} F(\bar{s}/\bar{u}) F(\bar{x}/\bar{u}) \frac{d\bar{u}}{\bar{u}}, \tag{5}$$

where $\bar{u}$ is a dimensionless integration variable, and $F(y)$ is an expression proportional to the stress intensity factor for a cracked body under a point load at normalized location, y. An approximate expression of $F(y)$ has been obtained by fitting a numerical solution, as (Murakami, 1986)

$$\begin{aligned} F(y) &= \left[1 + (1-y^2) \sum_{n=0}^{4} \alpha_{2n} y^{2n} \right] / \sqrt{1-y^2} \\ &= [1 + (1-y^2)(0.2945 - 0.3912y^2 + 0.7685y^4 - 0.9942y^6 + 0.5094y^8)] / \sqrt{1-y^2}, \end{aligned} \tag{6}$$

where α_0, α_2, α_4, α_6, and α_8 are the coefficients in the approximate expression of stress intensity factor.

Through tedious derivations and by integrating by parts (see Appendix B), Equation (2a) can be re-arranged as

$$\bar{H}(\bar{x}, \bar{t}) = -\frac{8}{\pi} I_\gamma(0) \bar{p}(\bar{x}_0, \bar{t}) \bar{x} I_\eta(\bar{x}) - \frac{8}{\pi} \int_0^1 \int_{max(\bar{s}, \bar{x})}^{1} F(\bar{x}/\bar{u}) I_\gamma(\bar{s}/\bar{u}) \bar{p}'(\bar{s}, \bar{t}) d\bar{u} d\bar{s}, \tag{7}$$

where $\bar{p}'(\bar{s}, \bar{t}) = \partial \bar{p}(\bar{s}, \bar{t}) / \partial \bar{s}$ is the dimensionless pressure gradient in the crack, and the two integrals, $I_\gamma(y)$ and $I_\eta(y)$, are given as,

$$\begin{cases} I_\gamma(y) = \int_1^y F(z) dz \\ I_\eta(y) = -\int_1^y \frac{F(z)}{z^2} dz \end{cases} \tag{8}$$

The two equations, Equations (1a) and (7), can then be used to solve for two unknown functions, $\bar{H}(\bar{x}, \bar{t})$ and $\bar{p}(\bar{x}, \bar{t})$.

The boundary conditions are such that the pressure history at the crack mouth is prescribed, the crack opening displacement at the crack tip is zero, and the pressure gradient at the crack tip is zero since there is no net flow into or out of the crack tip, i.e.,

$$\begin{cases} \bar{p}(\bar{x}_0, \bar{t}) = \bar{p}_0(\bar{t}) \\ \bar{H}(1, \bar{t}) = 0 \\ \partial\bar{p}/\partial\bar{x}|_{\bar{x}=1} = 0 \end{cases}, \tag{9}$$

where, for a realistic rolling contact problem, $\bar{p}_0(\bar{t})$ is determined by the pressure profile underneath the roller and the speed of the roller.

The initial condition can be chosen rather arbitrarily, such as that the initial pressure is zero everywhere in the crack. The choice of initial condition will slightly affect the transient solution and will have no effect on the steady state solution.

3. Numerical Method

It is clear that the governing equations of this problem are highly nonlinear, and involve complicated differential and integral calculations. An accurate solution inevitably requires numerical techniques. Here a numerical solution is attempted using finite difference method. A special interpolation technique and the solution method in the current study are described in this section.

3.1 Interpolation of the Unknown Quantities

A number of interpolation techniques for the pressure distribution within the crack have been tested. Some techniques would result in an oscillatory behavior or even unboundedness of the solutions. It was found that using a quadratic interpolation of the pressure distribution similar to that used by Houpert and Hamrock (1986), convergent solutions were readily obtained. Therefore a quadratic interpolation of the pressure distribution is used in the following. The crack opening displacement distribution is then expressed in terms of numerical values of the pressure distribution using Equation (7). The details of the interpolation scheme are given below.

Uniform division of the domain of interest, $\bar{x} \in [0, 1]$, is used in the computation with an even number of intervals N, the nodal coordinates $\bar{x}_j$ $(j = 0, 1, 2 \ldots N-1, N)$, and the corresponding nodal pressure values $\bar{P}_j = \bar{p}(\bar{x}_j, \bar{t})$ (although this approach can be easily extended to variable interval size formulation (Houpert and Hamrock, 1986) or multilevel interval size method by Venner et al (1990,1991)). The length of each interval is thus $1/N$. The N intervals are further grouped into $N/2$ sub-intervals, $[\bar{x}_{m-1}, \bar{x}_{m+1}]$, ($m$=1, 3, 5... N-3, N-1). The interpolation of the pressure distribution within each sub-interval is then given by,

$$\bar{p}_m(\bar{x}, \bar{t}) = \bar{p}(\bar{x}, \bar{t})|_{\bar{x} \in [\bar{x}_{m-1}, \bar{x}_{m+1}]} = A_m \bar{x}^2 + B_m \bar{x} + C_m, \tag{10}$$

where A_m, B_m, C_m are determined from the nodal pressure values, $\bar{P}_{m-1}, \bar{P}_m, \bar{P}_{m+1}$. Clearly, such interpolated pressure distribution is continuous throughout the domain of interest. And the pressure gradient, which needs to be evaluated to solve the governing equations, is piecewise continuous within each sub-interval, but discontinuous at the border nodes between sub-intervals.

Using the interpolation function, Eqn (10), the nodal values of the pressure gradient within the i-th sub-interval, $\bar{p}'_m(\bar{x}_{m-1}, \bar{t})$, $\bar{p}'_m(\bar{x}_m, \bar{t})$, and $\bar{p}'_m(\bar{x}_{m+1}, \bar{t})$, can be evaluated as,

$$\begin{cases} \bar{p}'_m(\bar{x}_{m-1}, \bar{t}) = (-1.5\bar{P}_{m-1} + 2\bar{P}_m - 0.5\bar{P}_{m+1})N \\ \bar{p}'_m(\bar{x}_m, \bar{t}) = -0.5(\bar{P}_{m-1} - \bar{P}_{m+1})N \\ \bar{p}'_m(\bar{x}_{m+1}, \bar{t}) = (0.5\bar{P}_{m-1} - 2\bar{P}_m + 1.5\bar{P}_{m+1})N \end{cases}, \tag{11}$$

Although these nodal values are unique at the mid-point of each sub-interval, the values at the border points, $\bar{p}'_m(\bar{x}_{m-1}, \bar{t})$ and $\bar{p}'_m(\bar{x}_{m+1}, \bar{t})$, are not necessarily equal to the pressure gradient values of the same point evaluated from the neighboring sub-intervals. In the present computation, a simple average of the border nodal values from the two neighboring sub-intervals was taken to be the nodal value of the border point. Therefore, the nodal values of the pressure gradient for interior points of the domain can be given by,

$$\begin{cases} \bar{P}'_j = \bar{p}'_j(\bar{x}_j, \bar{t}) & j \text{ is odd} \\ \bar{P}'_j = [\bar{p}'_{j-1}(\bar{x}_j, \bar{t}) + \bar{p}'_{j+1}(\bar{x}_j, \bar{t})]/2 & j \text{ is even} \end{cases}. \tag{12}$$

The values of the pressure gradient at the end nodes, $\bar{x}_0 = 0$ and $\bar{x}_N = 1$, require special treatment. In this study, they are evaluated by

$$\begin{cases} \bar{P}'_0 = \bar{p}'_1(\bar{x}_0, \bar{t}) = (-1.5\bar{P}_0 + 2\bar{P}_1 - 0.5\bar{P}_2)\, N \\ \bar{P}'_N = \bar{p}'_{N-1}(\bar{x}_N, \bar{t}) = (0.5\bar{P}_{N-2} - 2\bar{P}_{N-1} + 1.5\bar{P}_N)\, N \end{cases} . \tag{13}$$

From the no-flow boundary condition at the crack tip, Eqn (9), the nodal value of the pressure at the crack tip can be given in terms of the pressure values near the crack tip, as

$$\bar{P}_N = (4\bar{P}_{N-1} - \bar{P}_{N-2})/3 . \tag{14}$$

With the above interpolation of the pressure distribution, the nodal values of the crack opening displacement, $\bar{H}_i$, can be given by integrating the elastic response of the cracked body, Eqn (7), analytically. The result takes the form,

$$\begin{cases} \bar{H}_i = \sum_{j=0}^{N} \bar{h}_{ij} \bar{P}_j & i = 0, 1, 2 \ldots N-2, N-1 \\ \bar{H}_N = 0 \end{cases} , \tag{15}$$

where the components of the coefficient matrix, $\bar{h}_{ij}$, are given in Appendix C.

Since the nodal values of both pressure gradient and crack opening displacement can be expressed in terms of the nodal values of the pressure, the problem then becomes to determine pressure distribution for given initial and boundary conditions.

3.2 Solution Method

The time integration of the partial differential equation, Eqn (1a), is achieved using the finite difference method. For a given time increment, $\Delta\bar{t}$, the computational scheme is given by

$$\left[\bar{H}^3_{i+1} \left(\frac{\partial \bar{p}}{\partial \bar{x}}\right)_{i+1} - \bar{H}^3_{i-1} \left(\frac{\partial \bar{p}}{\partial \bar{x}}\right)_{i-1} \right]^{(n+1)} = \frac{2}{N\Delta\bar{t}} \left(\bar{H}_i^{(n+1)} - \bar{H}_i^{(n)}\right), \tag{16}$$

here a fully implicit Euler time integration is used, $\bar{H}_i^{(n)}$ denotes the opening displacement of node i at time step (n). All other quantities in the equation are evaluated at time step $(n+1)$.

Eqn (16) represents a system of non-linear algebraic equations of the unknown vector, $P = [\bar{P}_1, \bar{P}_2, \bar{P}_3 \ldots \bar{P}_{N-2}, \bar{P}_{N-1}]^T$. In our calculation, constant time steps were taken.

Iteration method was used to solve the non-linear algebraic equations. Iteration was considered to be convergent when the incremental correction of the nodal pressure values is within a prescribed error. The residuals of the equation, f_i, for a given step of iteration can be evaluated by taking the difference between the two sides of Eqn (16) as, for interior points,

$$f_i = [\bar{H}_{i-1}^3(-0.5\bar{P}_{i-3} + 2\bar{P}_{i-2} - 2\bar{P}_i + 0.5\bar{P}_{i+1})]^{(n+1)} + [\bar{H}_{i+1}^3(-0.5\bar{P}_{i+3} + 2\bar{P}_{i+2} - 2\bar{P}_i + 0.5\bar{P}_{i-1})]^{(n+1)} - \frac{4(\bar{H}_i^{(n+1)} - \bar{H}_i^{(n)})}{N^2\Delta\bar{t}} \qquad i \text{ is odd}, \quad (17a)$$

$$f_i = [\bar{H}_{i-1}^3(\bar{P}_{i-2} - \bar{P}_i) + \bar{H}_{i+1}^3(\bar{P}_{i+2} - \bar{P}_i)]^{(n+1)} - \frac{4(\bar{H}_i^{(n+1)} - \bar{H}_i^{(n)})}{N^2\Delta\bar{t}} \qquad i \text{ is even}; \quad (17b)$$

and for boundary points,

$$f_1 = [\bar{H}_0^3(-3\bar{P}_0 + 4\bar{P}_1 - \bar{P}_2)]^{(n+1)} + [\bar{H}_2^3(-0.5\bar{P}_4 + 2\bar{P}_3 - 2\bar{P}_1 + 0.5\bar{P}_0)]^{(n+1)} - \frac{4(\bar{H}_1^{(n+1)} - \bar{H}_1^{(n)})}{N^2\Delta\bar{t}}, \quad (17c)$$

$$f_{N-1} = [\bar{H}_{N-2}^3(-0.5\bar{P}_{N-4} + 2\bar{P}_{N-3} - 2\bar{P}_{N-1} + 0.5\bar{P}_N)]^{(n+1)} - \frac{4(\bar{H}_{N-1}^{(n+1)} - \bar{H}_{N-1}^{(n)})}{N^2\Delta\bar{t}}, \quad (17d)$$

here again the superscript $(n+1)$ represents the quantities evaluated at time step $(n+1)$. The residual vector can be denoted as $F = [f_1, f_2, f_3, \ldots f_{N-2}, f_{N-1}]^T$ which is a function of the pressure vector P.

So the problem becomes to determine, for each time step, the $N-1$ unknowns, P, which satisfy the $N-1$ equations $F(P) = 0$ and the boundary condition, $\bar{P}_0 = \bar{p}_0(\bar{t})$.

A modified Newton-Raphson iteration method was used to search the roots of the nonlinear algebraic equations,

$$F(P_{(k+1)}) = \alpha F(P_{(k)}) + \partial F(P_{(k)})(P_{(k+1)} - P_{(k)}) = 0 \tag{18}$$

where the subscript k is the iteration number and α is a relaxation factor which is equal to or smaller than unity, $\partial F(P_{(k)})$ is the Jacobian evaluated at iteration step (k), as

$$\partial F(P_{(k)}) = \begin{bmatrix} \frac{\partial f_1}{\partial \bar{P}_1} & \frac{\partial f_1}{\partial \bar{P}_2} & \frac{\partial f_1}{\partial \bar{P}_3} & \cdots & \frac{\partial f_1}{\partial \bar{P}_{N-1}} \\ \frac{\partial f_2}{\partial \bar{P}_1} & \frac{\partial f_2}{\partial \bar{P}_2} & \frac{\partial f_2}{\partial \bar{P}_3} & \cdots & \frac{\partial f_2}{\partial \bar{P}_{N-1}} \\ \cdots & \cdots & & \cdots & \\ \frac{\partial f_{N-1}}{\partial \bar{P}_1} & \frac{\partial f_{N-1}}{\partial \bar{P}_2} & \frac{\partial f_{N-1}}{\partial \bar{P}_3} & \cdots & \frac{\partial f_{N-1}}{\partial \bar{P}_{N-1}} \end{bmatrix}. \tag{19}$$

Gaussian elimination method was used to solve the algebraic equations. Convergent solution was considered to be found when the following criterion was satisfied,

$$\sum_{j=1}^{N-1} \left| \bar{P}_{j(k+1)}^{(n+1)} - \bar{P}_{j(k)}^{(n+1)} \right| \Big/ \sum_{j=1}^{N-1} \left| \bar{P}_{j(k+1)}^{(n+1)} \right| < \varepsilon, \tag{20}$$

where $\varepsilon = 0.001$ is the error limit for the incremental correction of nodal pressure values. This criterion means that when an additional iteration from (k) to (k+1) does not result in any significant correction of the pressure distribution, we considered the iteration converged.

To avoid unreasonable results, an additional constraint on the solution — cavitation condition was introduced (Elrod, 1981). This condition requires that the pressure values can never go below zero, i.e.,

$$\bar{P}_j \geq 0, \ (j = 0, 1, 2, \ldots N-1, N). \tag{21}$$

When the pressure values have a tendency to drop below zero, nucleation of air cavities in the fluid would maintain the pressure level at zero. In our calculation, the nodal pressure values were manually set to zero during each iteration step whenever a negative pressure value appeared.

4. Examples and Discussion

A few typical numerical examples are given here to demonstrate the solution method in solving the complicated governing equations. The initial condition for all examples is that the pressure is zero everywhere within the crack. Both the transient and the steady state solutions will be sought. Some features of the solution will be discussed.

Fig. 3 shows a typical transient solution of the pressure distribution at several different instants under a crack-mouth cyclic loading of sinusoidal wave. The insert above the plot represents the applied loading history with the time instants at which the pressure distributions are given labeled. The time is measured in terms of the number of time steps $n = \bar{t}/\Delta\bar{t}$. It is clear from Fig. 3 that, upon applied cyclic loading at the crack mouth, the pressure is gradually transmitted into the crack. Eventually, the pressure at the crack tip may reach the same magnitude as the applied pressure at the crack mouth. This whole process represents the transient response of the fluid-solid system to external loading. The length of the transient stage depends on the viscosity of the fluid, the elastic property of the solid, the loading frequency, and perhaps the loading amplitude. For the particular loading frequency and material properties used in this simulation, a steady state is gradually reached after 5-6 cycles of loading. It is also noteworthy that, since cavitation condition was used in the computation, the calculated pressure level in the crack is never below zero.

There are two convergency issues involved in the solution: one concerns the spatial resolution for which sufficiently fine spatial grid must be chosen; the other concerns the errors caused by time integration of differential equations. Since fully implicit Newton-Raphson iteration scheme is employed, the integration error should not be accumulative as long as convergent solution can be obtained. To ensure sufficiently fine finite difference mesh for the solution, solutions using a few different grids were compared. Figures 4a-b show the solutions of pressure distribution using the mesh size of N=8, 64, and 128 at different instants during cyclic loading. Figure 4a shows the pressure distributions at different moments for N=8 and N=128, whereas Fig. 4b shows the distributions at one particular moment for several grid sizes. During transient stage, there is clear difference between the fine mesh and the coarse mesh. But the difference diminishes once the steady state is reached. Figures 4a-b also show that a mesh size of N=128 is adequate to reach a convergent solution for the given loading condition. Therefore, a mesh size of N=128 was used throughout the rest of the calculations.

To study the effect of the magnitude of time step on the convergence of the solution, three time increment sizes, $\Delta\bar{t}$ (=$\Delta t/\tau$), were used and the results were compared. Figure 5 shows the pressure distribution at three different instants during cyclic loading using three time step magnitudes. The figure indicates that the result using $\Delta\bar{t} = 136000$ (Curve A in Fig. 5) has noticeable difference from the ones using $\Delta\bar{t} = 13600$ (B in Fig. 5) and $\Delta\bar{t} = 6800$ (C in Fig. 5). However, when the magnitude of time increment is smaller than 13600, convergent solutions are obtained.

Fig. 6 shows the pressure distribution upon application of a step function loading at the crack mouth. This example is used to demonstrate two points. First, the result clearly shows that our computation algorithm is very stable. Even for a rapid changing loading such as a step function loading, a well behaved solution can be obtained readily with the present numerical technique. Second, the result indicates that, as predicted by the approximate solution by Hsia and Xu (1996), there exists a characteristic penetration time for the fluid-solid system. When the length of the loading period is shorter than the characteristic time, the pressure change at the crack mouth can not be transmitted deep into the crack. On the other hand, if the length of the loading period is longer than the characteristic time, a steady state pressure distribution is reached within the crack. It is also noted that near the crack tip, the solution exhibits small oscillation. The mechanism for developing oscillatory behavior in numerical solutions was discussed by Okamura (1982). In our solution, the oscillation is too small to cause concern.

The steady state pressure distribution within the crack upon cyclic pressure loading of sinusoidal wave is shown in Figure 7. The pressure distribution in the crack repeats itself completely upon each cycle of loading. However, the pressure build-up in the crack exhibits a phase shift from the applied pressure loading. When the applied pressure loading reaches the peak at $n = \bar{t}/\Delta\bar{t} = 550$, e.g., the pressure level deep in the crack is near its lowest level; whereas when the applied loading reaches its valley, the pressure deep in the crack is near its maximum level which is close to the peak level of the applied loading. This phase shift will result in a delay in the stress intensity experienced at the crack tip, which may affect the fracture behavior. The effect of pressure loading on the crack tip stress intensity will be discussed in a separate paper.

The crack opening displacement profiles at several different loading stages are plotted in Figure 8. Generally, these profiles are similar in shape. All of them have the asymptotic shape of $\sqrt{1-\bar{x}}$ near the crack tip. However, during the rising phase of the applied loading (n= 530~550),

the slope of the crack opening profile seems to be steeper than that during the falling phase (n= 570~600). The crack opening profile almost flattens out when the minimum applied loading level is reached at $\bar{t} = 600$. This can be easily explained by the pressure distribution patterns in Figure 7. During the rising phase of the applied loading, although the pressure is high near the crack mouth, the pressure near the crack tip is rather low, resulting in a steeper slope of the crack opening profile. But during the falling phase, a high pressure level near the crack tip and the minimum pressure at the crack mouth result in a flattened out crack opening profile. This result is very similar in nature to the crack opening profiles obtained by our approximate solution (see Hsia and Xu, 1996).

5. Concluding Remarks

The present work presents a model of the surface crack propagation under hydraulic pressure loading at the crack mouth, a mechanism believed to be responsible for material degradation in rolling contact components. A simplified case has been considered here, in which the fluid filling the crack was assumed to be Newtonian and incompressible, and the solid was considered to be linear elastic with a surface crack perpendicular to the contacting surface. The governing equations were found to be two coupled, non-linear integral/differential equations.

Finite difference method has been employed to solve the complicated governing equations. Within each time step, Newton-Raphson iteration was used to search for the roots of the non-linear algebraic equations. It was found that the interpolation of the unknown pressure distribution had significant effect on the convergence of the solution. Using a quadratic interpolation of the pressure distribution, a satisfactory, convergent solution was obtained. A few numerical examples were given which showed that the complete solution consisted of a transient stage followed by a steady state stage. During the transient stage, the pressure at the crack mouth is gradually transmitted into the crack until approximately the characteristic penetration time is reached. Once the steady state is reached, the pressure distribution in the crack either completely repeats itself when the applied pressure loading is cyclic, or uniform if a constant pressure is applied.

The present method can be used to study the crack propagation behavior under hydraulic pressure loading. For this the crack tip stress intensity factor must be evaluated for different types of loading. This is currently being pursued by the authors. Moreover, many assumptions in the

present model may not true in real rolling contact problems. More realistic cases may also be dealt with using the present framework with proper modifications.

Acknowledgment

The work has been supported by the Air Force Office of Scientific Research through grant No. F49620-93-1-0241. The authors would like to thank Profs. K.-C. Hwang and T.G. Shawki and Dr. D.-Y. Hua for helpful discussions.

References

Ai, X. and Zhang, L., "A General Model for Microelastohydrodynamic Lubrication and Its Full Numerical Solution", *ASME Journal of Tribology*, 111, pp. 569-576 (1989).

Bower, A. F., "The Influence of Crack Face Friction and Trapped Fluid on Surface Initiated Rolling Contact Fatigue Cracks", *ASME Journal of Tribology*, 110, pp. 704-711 (1988).

Bueckner, H. F., "A Novel Principle for the Computation of Stress Intensity Factors", *Zeitschrift fur Angewandte Mathematik und Mechanik*, 50, pp. 529-546 (1970).

Chang, L., Conry, T. I. and Cusano, C., "An Efficient Robust Multi-Level Computational Algorithm for Elastohydrodynamic Lubrication", *ASME Journal of Tribology*, 111, pp. 193-199 (1989a).

Chang, L., Cusano C. & Conry, T. F., "Effects of Lubricant Rheology and Kinematic Conditions on Micro-Elastohydrodynamic Lubrication", *ASME Journal of Tribology*, Vol. 111, No. 2, pp. 344-351 (1989b).

Clarke, T. M., Miller, G. R., Keer, L. M. and Cheng, H. S., "The Role of Near-Surface Inclusions in the Pitting of Gears", *ASLE Transactions*, 28, pp. 111-116 (1985).

Elrod, E. G., "A Cavitation Algorithm", *ASME Journal of Tribology*, 103, pp. 350-354 (1981).

Houpert, L. G. and Hamrock, B. J., "Fast Approach for Calculating Film Thicknesses and Pressures in Elastohydrodynamically Lubricated Contacts at High Loads", *ASME Journal of Tribology*, 108, pp. 411-420 (1986).

Hsia, K. J. and Xu, Z.-Q., "The Mathematical Framework and an Approximate Solution of Surface Crack Propagation under Hydraulic Pressure Loading", *Int. J. Fract.*, in press (1996).

Johnson, K. L., *Contact Mechanics*, Cambridge University Press (1985).

Kaneta, M. and Murakami, Y., "Effects of Oil Pressure on Surface Crack Growth in Rolling/Sliding Contact", *Tribology Int.*, 20, pp. 210-217 (1987).

Michau, B., Berthe, D. and Godet, M., "Observations of Oil Pressure Effects in Surface Crack Development", *Tribology Int.*, 7, pp. 119-122 (1974).

Murakami, Y. (ed.), *Stress Intensity Factors Handbook*, Pergamon, Oxford (1986).

Okamura, H., "A Contribution to the Numerical Analysis of Isothermal Elasto-Hydrodynamic Lubrication", *Proc. 9th Lees-Lyon Symposium on Tribology*, Leeds, 1982, Dowson, D. and Taylor, C.M. (Editors), IPC Science and Technology, Guildford, pp. 313-320 (1984).

Osborn, K. F. and Sadeghi, F., "Time Dependent Line EHD Lubrication Using the Multigrid/ Multilevel Technique", *ASME Journal of Tribology*, 114, pp. 68-74 (1992).

Srivatsan,T. S. and Sudarshan, T. S., "Review: Mechanisms of Fatigue Crack Initiation in Metals: Role of Aqueous Environments," *J. Mater. Sci.*, 23, pp. 1521-1533 (1988).

Suh, N. P., *Tribophysics*, Prentice-Hall, Inc., Englewood Cliffs, NJ (1986).

Tada, H., Paris, P. C. and Irwin, G. R. (ed.), *The Stress Analysis of Cracks Handbook*, Paris Production Inc., St. Louis (1985).

Tzou, J.-L., Suresh, S. and Ritchie, R. O., "Fatigue Crack Propagation in Oil Environments - I: Crack Growth Behavior in Silicone and Paraffin Oils," *Acta metall.*, 33, pp. 105-116 (1985a).

Tzou, J.-L., Hsueh, C. H., Evans, A. G. and Ritchie, R. O., "Fatigue Crack Propagation in Oil Environments - II: a Model for Crack Closure Induced by Viscous Fluids", *Acta metall.*, 33, pp. 117-127 (1985b).

Venner, C. H. and Lubrecht, A. A., "Transient Analysis of Surface Features in an EHL Line-Contact in the Case of Sliding", *ASME Journal of Tribology*, 116, pp. 186-193 (1994).

Venner, C. H., Lubrecht, A. A. and ten Napel, W. E., "Numerical Simulation of the Over-rolling of a Surface Feature in an EHL Line Contact", *ASME Journal of Tribology*, 113, pp. 777-783 (1991).

Venner, C. H., ten Napel, W.E. and Bosma, R., "Advanced Multilevel Solution of the EHL Line Contact Problem", *ASME Journal of Tribology*, 112, pp. 426-432 (1990).

Way, S., "Pitting due to Rolling Contact", *J. Appl. Mech., Trans. ASME*, 2, A49-58 (1935).

Appendix A: Green's Function

From Castigliano's theorem, the displacement Δ_x caused by a load Q (in the loading direction) at location x may be computed by

$$\Delta_x = \frac{\partial U_T}{\partial Q}, \tag{A1}$$

where U_T is the total strain energy. U_T maybe regarded as that due to applying forces on a configuration without crack plus that due to introducing the crack a while holding forces constant (Tada, et al, 1985),

$$U_T = U_{NoCrack} + \int_0^a \tilde{G} da \tag{A2}$$

where $\tilde{G}$ is the energy release rate. If only opening mode (Mode I) displacement is considered, $\tilde{G}$, can be written as

$$E'\tilde{G} = (K_{IP} + K_{IQ})^2 \tag{A3}$$

where K_{IP} and K_{IQ} are the Mode I stress intensity factors due to forces P and virtual forces Q, respectively. Following the same steps as in Tada, et al (1985), the opening displacement of the crack surface under a pair of concentrated forces, Q, at $x = a_Q$ can be given as

$$\Delta_x = \frac{2}{E'} \int_{a_Q}^{a} K_{IP} \frac{\partial K_{IQ}}{\partial Q} da. \tag{A4}$$

The Mode I stress intensity factor K_{IP} can be written as

$$K_{IP} = \begin{cases} \dfrac{2P}{\sqrt{\pi a}} F(x/a) & x < a \\ 0 & x \geq a \end{cases} \tag{A5}$$

where a is the length of the crack. Substituting (A5) into (A4), we obtain the opening displacement $\Delta_x(s, t)$ at location x due to a pair of concentrated forces P at location s,

$$\Delta_x(s, t) = \frac{8P(s, t)}{\pi E'} \int_{max\{x, s\}}^{a} F(s/u)F(x/u)\frac{du}{u}. \tag{A6}$$

Based on linear elastic fracture mechanics, the opening displacement $H(x, t)$ at location x due to the pressure distribution $p(s, t)$ can then be written as

$$H(x, t) = \int_0^a \Delta_x(s, t)ds = \int_0^a \frac{8p(s, t)}{\pi E'} \int_{max\{x, s\}}^{a} F(s/u)F(x/u)\frac{du}{u}ds. \tag{A7}$$

With proper normalization, we obtain the expression for the Green's function in Equation (5).

Appendix B: Derivation of Equation (7)

Substitute Equation (5) into Equation (2a), we have

$$\bar{H}(\bar{x}, \bar{t}) = \int_0^1 \frac{8}{\pi} \int_{max(\bar{s}, \bar{x})}^1 F(\bar{s}/\bar{u}) F(\bar{x}/\bar{u}) \frac{d\bar{u}}{\bar{u}} \bar{p}(\bar{s}, \bar{t}) d\bar{s}$$

$$= \frac{8}{\pi} \int_{\bar{x}}^1 F(\bar{x}/\bar{u}) \int_0^{\bar{u}} F(\bar{s}/\bar{u}) \bar{p}(\bar{s}, \bar{t}) \frac{d\bar{s}}{\bar{u}} d\bar{u} \quad . \tag{B1}$$

Integrating the inner integration by part, we obtain,

$$\bar{H}(\bar{x}, \bar{t}) = \frac{8}{\pi} \int_{\bar{x}}^1 F(\bar{x}/\bar{u}) \left[I_\gamma(\bar{s}/\bar{u}) \bar{p}(\bar{s}, \bar{t}) \Big|_{\bar{s}=0}^{\bar{s}=\bar{u}} - \int_0^{\bar{u}} I_\gamma(\bar{s}/\bar{u}) \frac{\partial}{\partial \bar{s}} \bar{p}(\bar{s}, \bar{t}) d\bar{s} \right] d\bar{u}$$

$$= \frac{8}{\pi} \int_{\bar{x}}^1 F(\bar{x}/\bar{u}) \left[-I_\gamma(0) \bar{p}(0, \bar{t}) - \int_0^{\bar{u}} I_\gamma(\bar{s}/\bar{u}) \bar{p}'(\bar{s}, \bar{t}) d\bar{s} \right] d\bar{u} \quad . \tag{B2}$$

Re-arranging the last expression and the integration limits in (B2), we can then obtain Equation (7).

Appendix C: Detailed Derivation of Elasticity Coefficient, $\bar{h}_{ij}$, in Equation (15)

From Equation (7), the opening displacement at location $\bar{x}_i$, $\bar{H}_i = \bar{H}(\bar{x}_i, \bar{t})$, can be evaluated as,

$$\bar{H}_i = \bar{H}(\bar{x}_i, \bar{t}) = -\frac{8}{\pi} I_\gamma(0)\bar{x}_i I_\eta(\bar{x}_i)\bar{p}(\bar{x}_0, \bar{t}) - \frac{8}{\pi}\int_0^1 \int_{max(\bar{s}, \bar{x}_i)}^1 F(\bar{x}_i/\bar{u}) I_\gamma(\bar{s}/\bar{u})\bar{p}'(\bar{s}, \bar{t}) d\bar{u} d\bar{s}$$

$$= -\frac{8}{\pi} I_\gamma(0)\bar{x}_i I_\eta(\bar{x}_i)\bar{p}(\bar{x}_0, \bar{t}) - \frac{8}{\pi} \sum_{m=1,3,5\ldots}^{N-1} \int_{\bar{x}_{m-1}}^{\bar{x}_{m+1}} \int_{max(\bar{s}, \bar{x}_i)}^1 F(\bar{x}_i/\bar{u}) I_\gamma(\bar{s}/\bar{u})\bar{p}'_m(\bar{s}, \bar{t}) d\bar{u} d\bar{s} \quad \text{(C1)}$$

Utilizing the interpolation functions for pressure gradient, Equation (12), the integrand can be given in terms of the nodal values of the pressure distribution, as

$$\bar{H}_i = 4\gamma_0 \bar{x}_i I_\eta(\bar{x}_i)\bar{P}_0 - \frac{8}{\pi} \sum_{m=1,3,5\ldots}^{N-1} \int_{max(\bar{x}_i, \bar{x}_{m-1})}^1 F(\bar{x}_i/\bar{u}) \int_{\bar{x}_{m-1}}^{min(\bar{u}, \bar{x}_{m+1})} I_\gamma(\bar{s}/\bar{u}) * N\left[N(\bar{P}_{m+1} - 2\bar{P}_m + \bar{P}_{m-1})(\bar{s} - \bar{x}_m) + \frac{N}{2}(\bar{P}_{m+1} - \bar{P}_{m-1})\right] d\bar{s} d\bar{u} \quad \text{(C2)}$$

Upon integration and re-arrangement, Equation (C2) can be expressed in terms of nodal pressure values as,

$$\bar{H}_i = 4\gamma_0 \bar{x}_i I_\eta(\bar{x}_i)\bar{P}_0 - \sum_{m=1,3,5\ldots}^{N-1} K_{im} N^2 (\bar{P}_{m+1} - 2\bar{P}_m + \bar{P}_{m-1}) - \sum_{m=1,3,5\ldots}^{N-1} M_{im}\left[\frac{N}{2}(\bar{P}_{m+1} - \bar{P}_{m-1}) - \bar{x}_m N^2 (\bar{P}_{m+1} - 2\bar{P}_m + \bar{P}_{m-1})\right] \quad \text{(C3)}$$

where K_{im} and M_{im} are integrals given by,

$$\begin{cases} K_{im} = \int_{max\{\bar{x}_i, \bar{x}_{m+1}\}}^1 \frac{8}{\pi} F(\bar{x}_i/\bar{u}) I_\xi(\bar{x}_{m+1}/\bar{u})\bar{u}^2 d\bar{u} - \int_{max\{\bar{x}_i, \bar{x}_{m-1}\}}^1 \frac{8}{\pi} F(\bar{x}_i/\bar{u}) I_\xi(\bar{x}_{m-1}/\bar{u})\bar{u}^2 d\bar{u} \\ M_{im} = \int_{max\{\bar{x}_i, \bar{x}_{m+1}\}}^1 \frac{8}{\pi} F(\bar{x}_i/\bar{u}) I_\zeta(\bar{x}_{m+1}/\bar{u})\bar{u} d\bar{u} - \int_{max\{\bar{x}_i, \bar{x}_{m-1}\}}^1 \frac{8}{\pi} F(\bar{x}_i/\bar{u}) I_\zeta(\bar{x}_{m-1}/\bar{u})\bar{u} d\bar{u} \end{cases} \quad \text{(C4)}$$

where the integrations can be carried out for the stress intensity factor function in Equation (6). The functions $I_\xi(y)$, $I_\zeta(y)$, $I_\gamma(y)$, and $I_\eta(y)$ are integrals given by,

$$
\begin{cases}
I_\xi(y) = \int_1^y I_\gamma(z)z\,dz = (\frac{\gamma_0}{2}y^2 + \xi_0)\,(\text{asin}y - \frac{\pi}{2}) + \sqrt{1-y^2}\sum_{n=0}^{5}\xi_{2n+1}y^{2n+1} \\
I_\zeta(y) = \int_1^y I_\gamma(z)dz = \gamma_0 y\,(\text{asin}y - \frac{\pi}{2}) + \sqrt{1-y^2}\sum_{n=0}^{5}\zeta_{2n+1}y^{2n} \\
I_\gamma(y) = \int_1^y F(z)dz = \gamma_0\,(\text{asin}y - \frac{\pi}{2}) + \sqrt{1-y^2}\sum_{n=0}^{4}\gamma_{2n+1}y^{2n+1} \\
I_\eta(y) = -\int_1^y F(z)\frac{dz}{z^2} = \eta_0\,(\text{asin}y - \frac{\pi}{2}) + \sqrt{1-y^2}\sum_{n=0}^{4}\eta_{2n+1}y^{2n-1}
\end{cases}
\tag{C5}
$$

where ξ_{2n+1}, ζ_{2n+1}, γ_{2n+1}, and η_{2n+1} are linear combinations of the coefficients in the expression of the stress intensity factor, α_{2n}, in Equation (6),

$$
\begin{cases}
\xi_0 = -\frac{\gamma_0}{4} + \frac{\gamma_1}{4\cdot 2} + \frac{3\cdot\gamma_3}{6\cdot 4\cdot 2} + \frac{5\cdot 3\cdot\gamma_5}{8\cdot 6\cdot 4\cdot 2} + \frac{7\cdot 5\cdot 3\cdot\gamma_7}{10\cdot 8\cdot 6\cdot 4\cdot 2} + \frac{9\cdot 7\cdot 5\cdot 3\cdot\gamma_9}{12\cdot 10\cdot 8\cdot 6\cdot 4\cdot 2} \\
\xi_1 = -\xi_0 \\
\xi_3 = \frac{\gamma_1}{4} - \frac{\gamma_3}{6\cdot 4} - \frac{5\cdot\gamma_5}{8\cdot 6\cdot 4} - \frac{7\cdot 5\cdot\gamma_7}{10\cdot 8\cdot 6\cdot 4} - \frac{9\cdot 7\cdot 5\cdot\gamma_9}{12\cdot 10\cdot 8\cdot 6\cdot 4} \\
\xi_5 = \frac{\gamma_3}{6} - \frac{\gamma_5}{8\cdot 6} - \frac{7\cdot\gamma_7}{10\cdot 8\cdot 6} - \frac{9\cdot 7\cdot\gamma_9}{12\cdot 10\cdot 8\cdot 6} \\
\xi_7 = \frac{\gamma_5}{8} - \frac{\gamma_7}{10\cdot 8} - \frac{9\cdot\gamma_9}{12\cdot 10\cdot 8} \\
\xi_9 = \frac{\gamma_7}{10} - \frac{\gamma_9}{12\cdot 10} \\
\xi_{11} = \frac{\gamma_9}{12}
\end{cases}
\tag{C5a}
$$

$$
\begin{cases}
\zeta_1 = \gamma_0 - \dfrac{\gamma_1}{3} - \dfrac{2\cdot\gamma_3}{5\cdot 3} - \dfrac{4\cdot 2\cdot\gamma_5}{7\cdot 5\cdot 3} - \dfrac{6\cdot 4\cdot 2\cdot\gamma_7}{9\cdot 7\cdot 5\cdot 3} - \dfrac{8\cdot 6\cdot 4\cdot 2\cdot\gamma_9}{11\cdot 9\cdot 7\cdot 5\cdot 3} \\
\zeta_3 = \dfrac{\gamma_1}{3} - \dfrac{\gamma_3}{5\cdot 3} - \dfrac{4\cdot\gamma_5}{7\cdot 5\cdot 3} - \dfrac{6\cdot 4\cdot\gamma_7}{9\cdot 7\cdot 5\cdot 3} - \dfrac{8\cdot 6\cdot 4\cdot\gamma_9}{11\cdot 9\cdot 7\cdot 5\cdot 3} \\
\zeta_5 = \dfrac{\gamma_3}{5} - \dfrac{\gamma_5}{7\cdot 5} - \dfrac{6\cdot\gamma_7}{9\cdot 7\cdot 5} - \dfrac{8\cdot 6\cdot\gamma_9}{11\cdot 9\cdot 7\cdot 5} \\
\zeta_7 = \dfrac{\gamma_5}{7} - \dfrac{\gamma_7}{9\cdot 7} - \dfrac{8\cdot\gamma_9}{11\cdot 9\cdot 7} \\
\zeta_9 = \dfrac{\gamma_7}{9} - \dfrac{\gamma_9}{11\cdot 9} \\
\zeta_{11} = \dfrac{\gamma_9}{11}
\end{cases}
\qquad \text{(C5b)}
$$

$$
\begin{cases}
\gamma_0 = 1 + \dfrac{\alpha_0}{2} + \dfrac{\alpha_2}{4\cdot 2} + \dfrac{3\cdot\alpha_4}{6\cdot 4\cdot 2} + \dfrac{5\cdot 3\cdot\alpha_6}{8\cdot 6\cdot 4\cdot 2} + \dfrac{7\cdot 5\cdot 3\cdot\alpha_8}{10\cdot 8\cdot 6\cdot 4\cdot 2} \\
\gamma_1 = \dfrac{\alpha_0}{2} - \dfrac{\alpha_2}{4\cdot 2} - \dfrac{3\cdot\alpha_4}{6\cdot 4\cdot 2} - \dfrac{5\cdot 3\cdot\alpha_6}{8\cdot 6\cdot 4\cdot 2} - \dfrac{7\cdot 5\cdot 3\cdot\alpha_8}{10\cdot 8\cdot 6\cdot 4\cdot 2} \\
\gamma_3 = \dfrac{\alpha_2}{4} - \dfrac{\alpha_4}{6\cdot 4} - \dfrac{5\cdot\alpha_6}{8\cdot 6\cdot 4} - \dfrac{7\cdot 5\cdot\alpha_8}{10\cdot 8\cdot 6\cdot 4} \\
\gamma_5 = \dfrac{\alpha_4}{6} - \dfrac{\alpha_6}{8\cdot 6} - \dfrac{7\cdot\alpha_8}{10\cdot 8\cdot 6} \\
\gamma_7 = \dfrac{\alpha_6}{8} - \dfrac{\alpha_8}{10\cdot 8} \\
\gamma_9 = \dfrac{\alpha_8}{10}
\end{cases}
\qquad \text{(C5c)}
$$

$$
\begin{cases}
\eta_0 = \alpha_0 - \dfrac{\alpha_2}{2} - \dfrac{\alpha_4}{4\cdot 2} - \dfrac{3\cdot\alpha_6}{6\cdot 4\cdot 2} - \dfrac{5\cdot 3\cdot\alpha_8}{8\cdot 6\cdot 4\cdot 2} \\
\eta_1 = 1 + \alpha_0 \\
\eta_3 = -\dfrac{\alpha_2}{2} + \dfrac{\alpha_4}{4\cdot 2} + \dfrac{3\cdot\alpha_6}{6\cdot 4\cdot 2} + \dfrac{5\cdot 3\cdot\alpha_8}{8\cdot 6\cdot 4\cdot 2} \\
\eta_5 = -\dfrac{\alpha_4}{4} + \dfrac{\alpha_6}{6\cdot 4} + \dfrac{5\cdot\alpha_8}{8\cdot 6\cdot 4} \\
\eta_7 = -\dfrac{\alpha_6}{6} + \dfrac{\alpha_8}{8\cdot 6} \\
\eta_9 = -\dfrac{\alpha_8}{8}
\end{cases}
\qquad \text{(C5d)}
$$

From the above derivations, the elasticity coefficients, $\bar{h}_{ij}$, in Equation (15) are given by,

$$\bar{h}_{ij} = 2N^2 (K_{ij} - \bar{x}_j M_{ij}) \qquad j = 1, 3, \ldots, N-1 \tag{C6a}$$

$$\bar{h}_{ij} = -N^2 K_{i,j-1} - (0.5N - \bar{x}_{j-1} N^2) M_{i,j-1} - N^2 K_{i,j+1} + (0.5N + \bar{x}_{j+1} N^2) M_{i,j+1}$$

$$j = 2, 4, \ldots, N-2 \tag{C6b}$$

For boundary nodes, $\bar{h}_{ij}$ are specially treated such that,

$$\begin{cases} \bar{h}_{i0} = -N^2 K_{i1} + (0.5N + \bar{x}_1 N^2) M_{i1} + 4\gamma_0 \bar{x}_i I_\eta(\bar{x}_i) \\ \bar{h}_{iN} = -N^2 K_{i,N-1} - (0.5N - \bar{x}_{N-1} N^2) M_{i,N-1} \end{cases} \tag{C7}$$

Figure Captions

Figure 1 Schematic of hydraulic pressure loading on a cracked body caused by a roller.

Figure 2 An idealized configuration considered in the model.

Figure 3 Pressure distribution within the crack during transient stage, the insert above the plot is the applied loading history at the crack mouth.

Figure 4 Convergency study for different spatial mesh size: (a) comparison of pressure distributions at several different times for two meshes (N=8, 128); (b) comparison of pressure distribution at a particular time for three meshes (N=8, 64, and 128).

Figure 5 Convergency study for different time increment: pressure distributions at several times using three different $\Delta\bar{t}$: $\Delta\bar{t} = 136000$ (curve A), $\Delta\bar{t} = 13600$ (curve B), and $\Delta\bar{t} = 6800$ (curve C).

Figure 6 Pressure distributions within the crack upon a step function loading at the crack mouth.

Figure 7 Steady state pressure distributions at different times within a loading cycle under cyclic pressure loading at the crack mouth.

Figure 8 Crack opening displacement profile during loading and unloading stages.

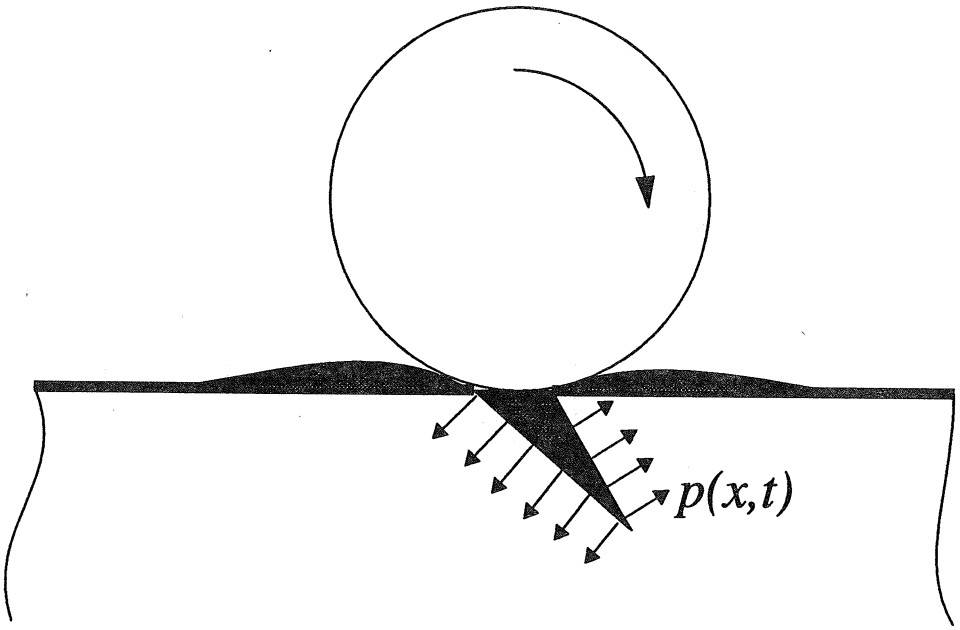

Figure 1

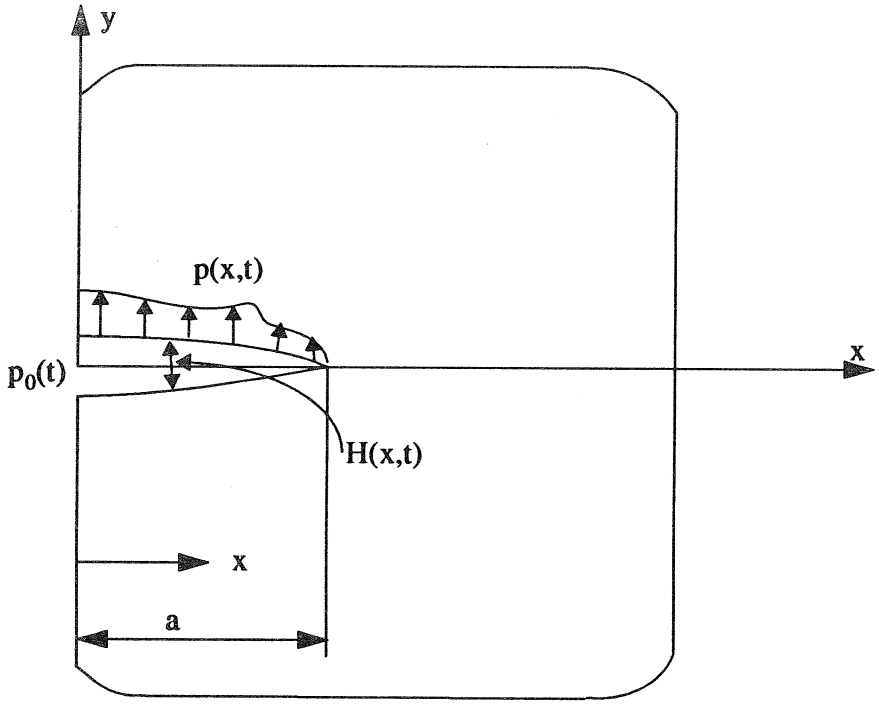

Figure 2

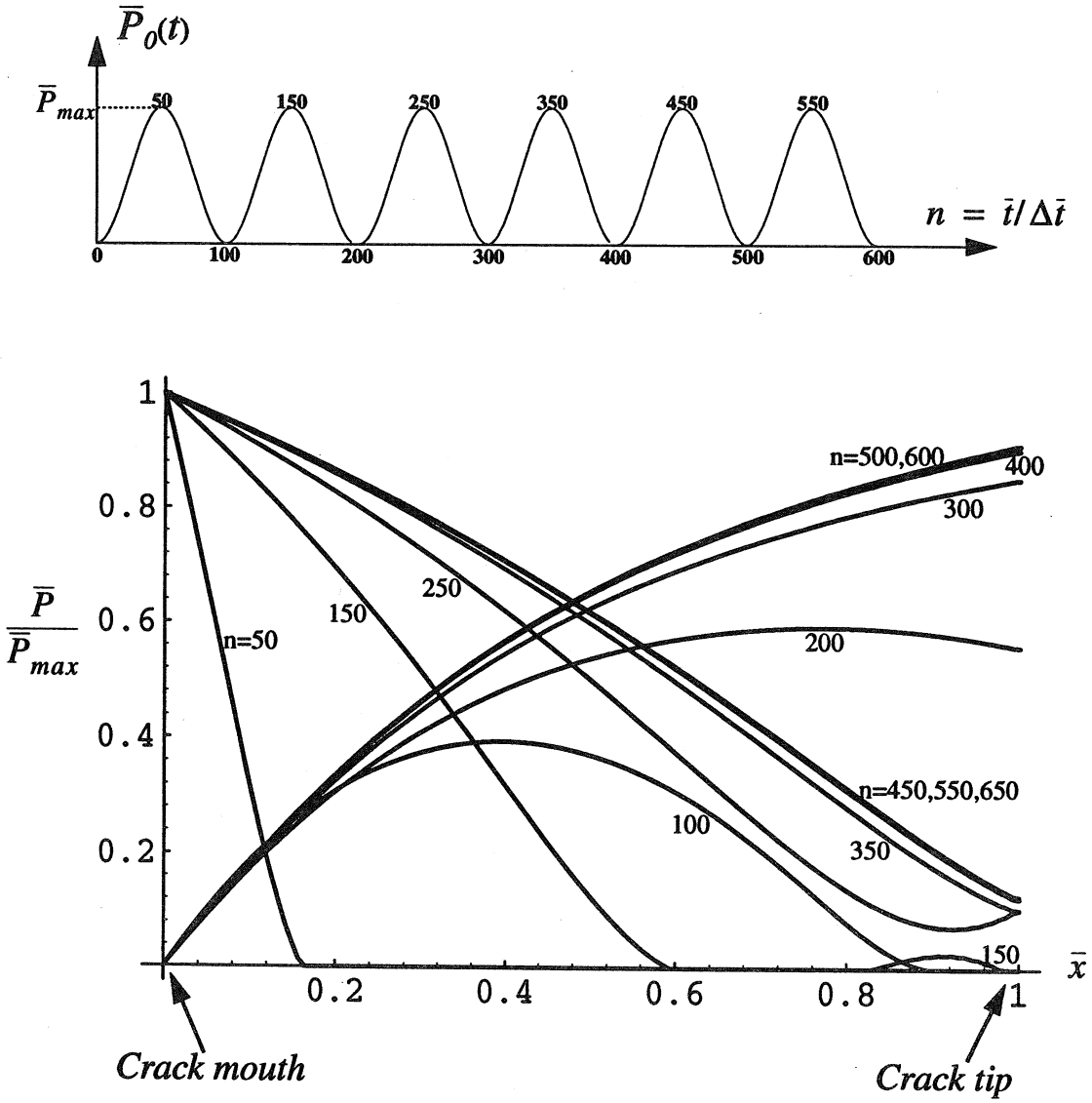
$\overline{P}_0(t)$
$\overline{P}_{max}$
50
150
250
350
450
550
0
100
200
300
400
500
600
$n = \bar{t}/\Delta\bar{t}$
1
0.8
0.6
0.4
0.2
$\frac{\overline{P}}{\overline{P}_{max}}$
n=500,600
400
300
250
150
n=50
200
n=450,550,650
100
350
150
0.2
0.4
0.6
0.8
1
$\bar{x}$
Crack mouth
Crack tip

Figure 3

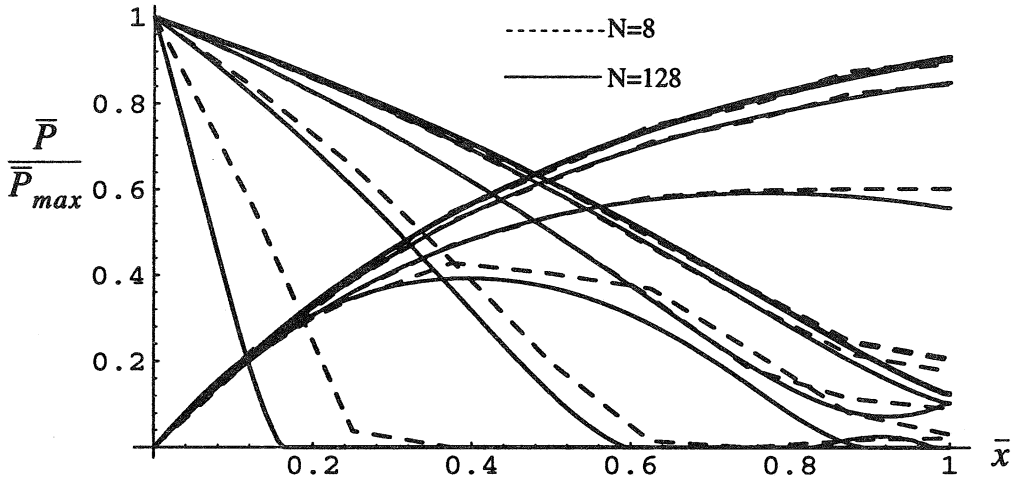
N=8
N=128
$\frac{\overline{P}}{\overline{P}_{max}}$
1
0.8
0.6
0.4
0.2
0.2
0.4
0.6
0.8
1
$\bar{x}$

(a)

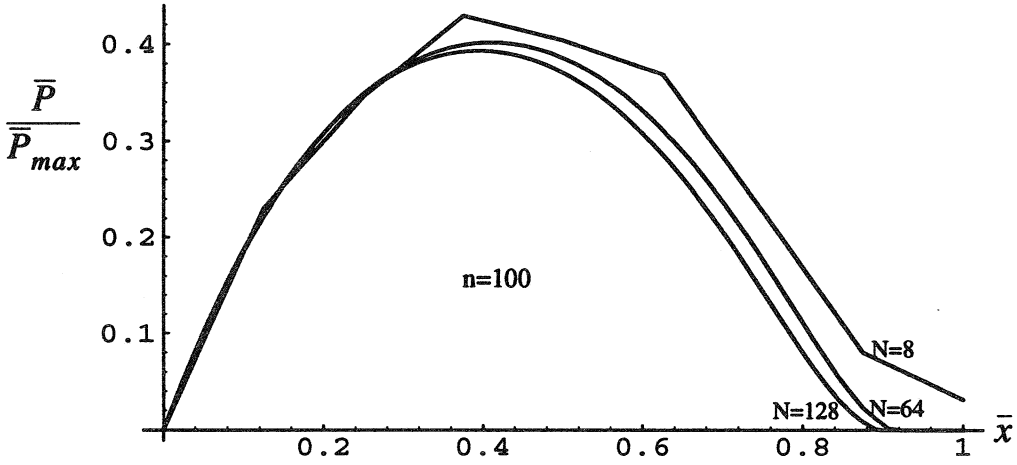
$\frac{\overline{P}}{\overline{P}_{max}}$
0.4
0.3
0.2
0.1
n=100
N=8
N=128
N=64
0.2
0.4
0.6
0.8
1
$\bar{x}$

(b)

Figure 4

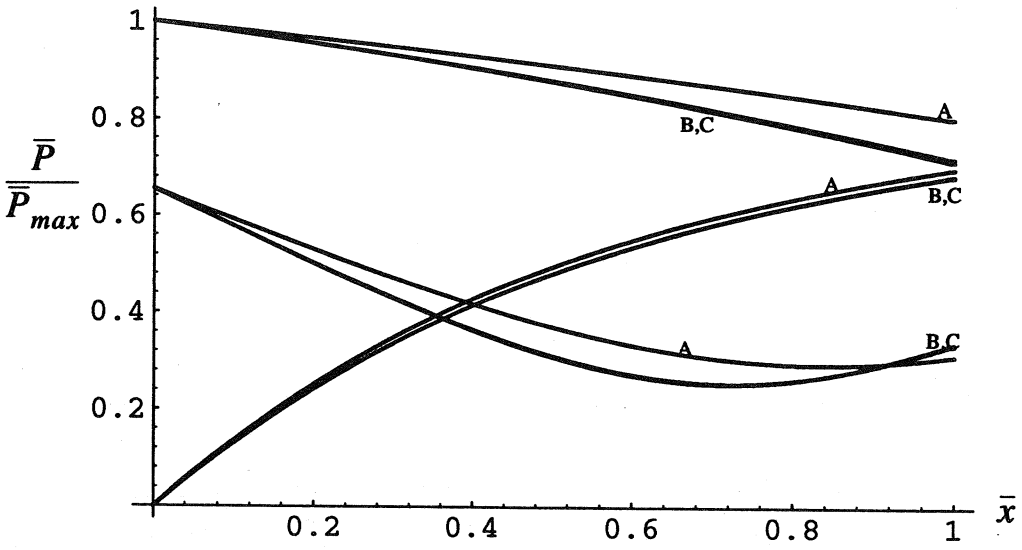
1
0.8
0.6
0.4
0.2
$\frac{\overline{P}}{\overline{P}_{max}}$
0.2
0.4
0.6
0.8
1
$\overline{x}$
A
B,C
A
B,C
A
B,C

Figure 5

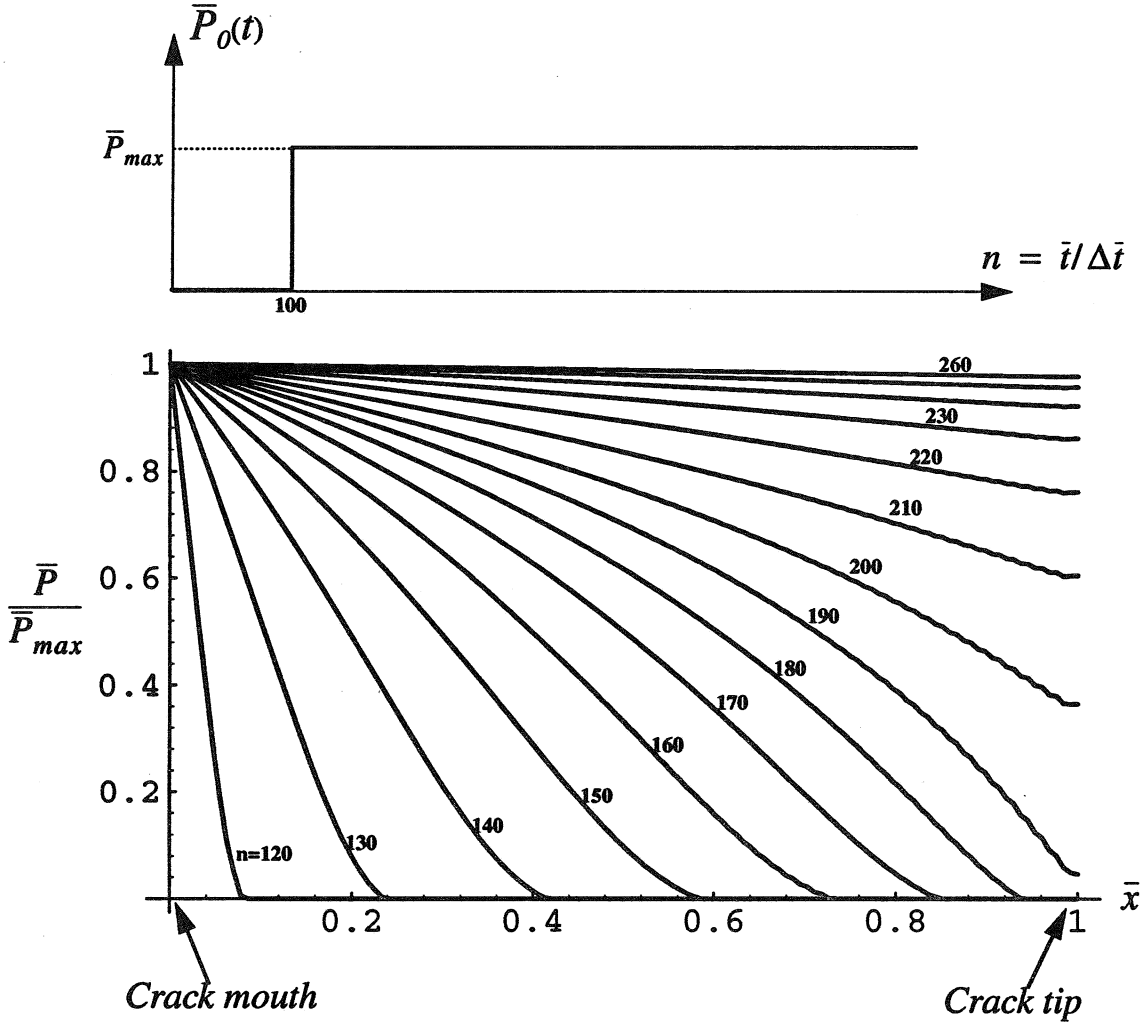
$\overline{P}_0(\bar{t})$
$\overline{P}_{max}$
$n = \bar{t}/\Delta\bar{t}$
100
1
0.8
0.6
0.4
0.2
$\frac{\overline{P}}{\overline{P}_{max}}$
260
230
220
210
200
190
180
170
160
150
140
130
n=120
0.2
0.4
0.6
0.8
1
$\bar{x}$
Crack mouth
Crack tip

Figure 6

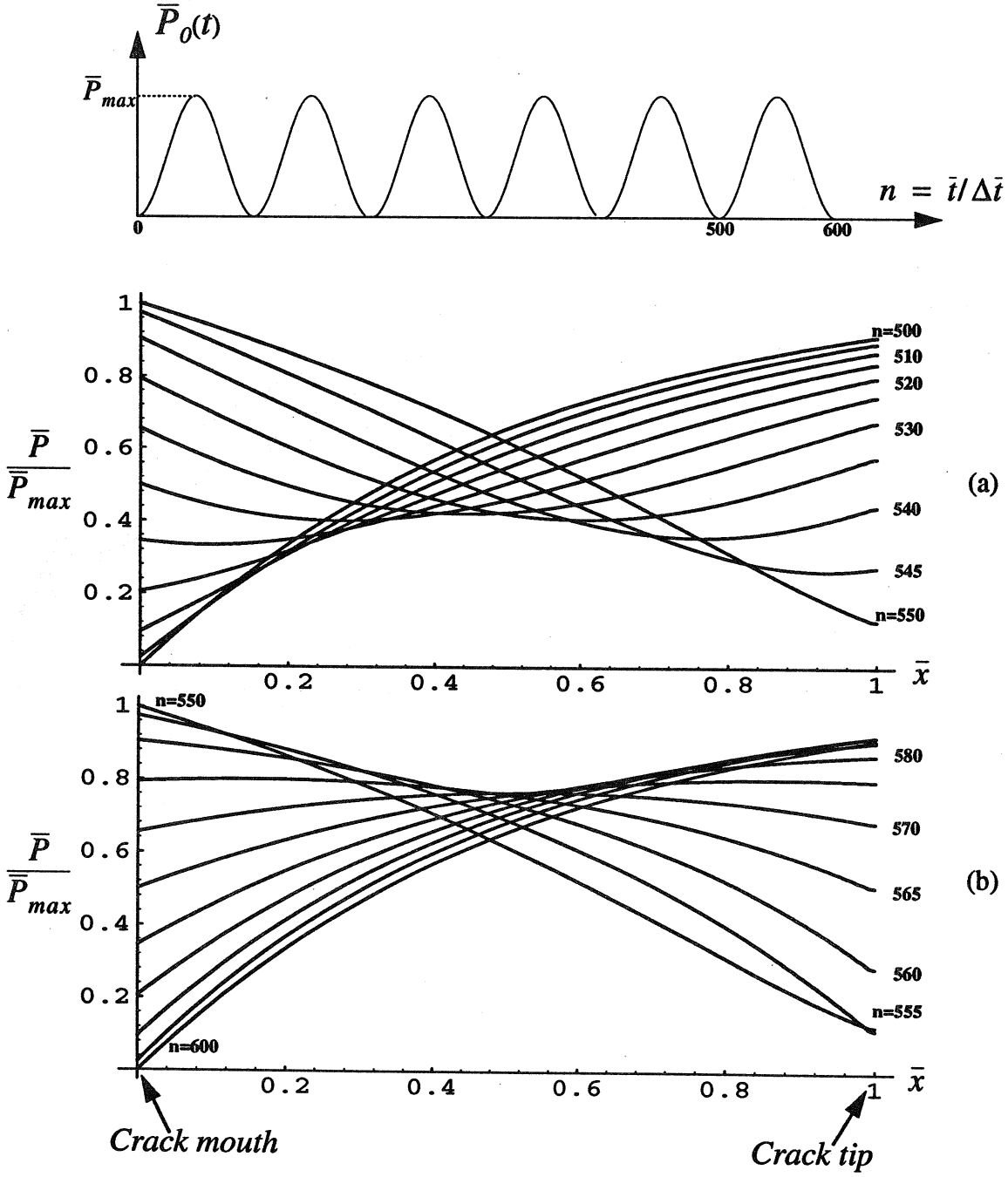
$\bar{P}_0(t)$
$\bar{P}_{max}$
$n = \bar{t}/\Delta\bar{t}$
0
500
600
$\frac{\bar{P}}{\bar{P}_{max}}$
1
0.8
0.6
0.4
0.2
n=500
510
520
530
540
545
n=550
0.2
0.4
0.6
0.8
1
$\bar{x}$
(a)
n=550
580
570
565
560
n=555
n=600
(b)
Crack mouth
Crack tip

Figure 7

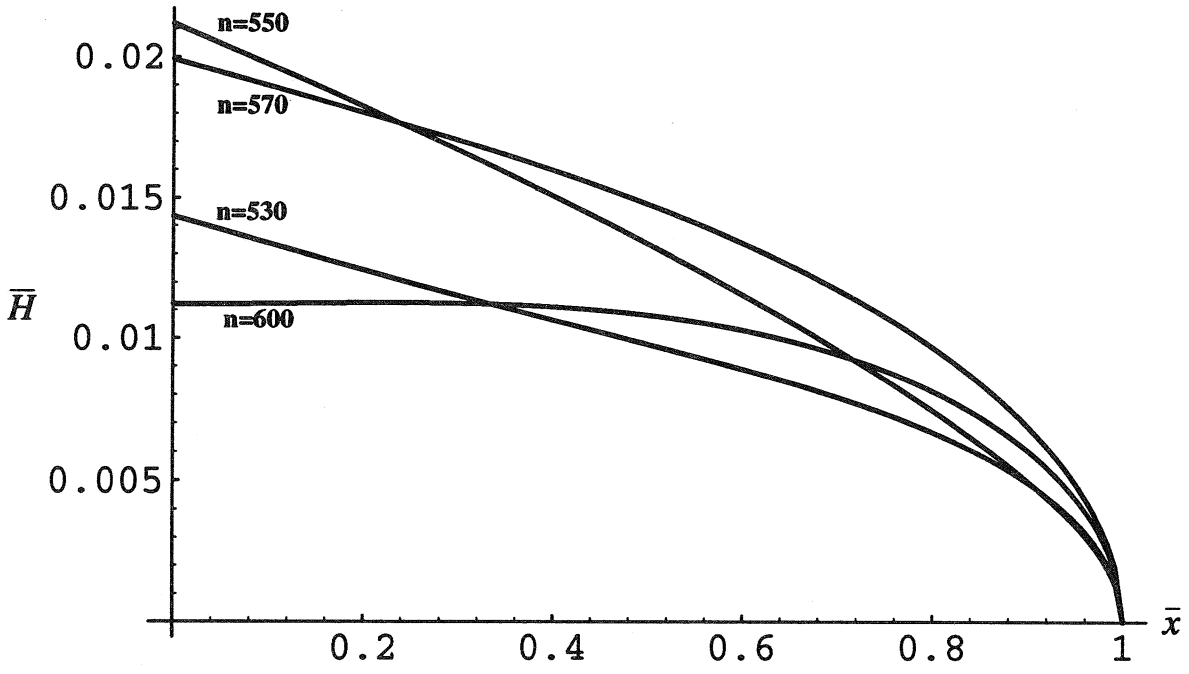
n=550
n=570
n=530
n=600
0.02
0.015
0.01
0.005
$\overline{H}$
0.2
0.4
0.6
0.8
1
$\bar{x}$

Figure 8

List of Recent TAM Reports

No.	Authors	Title	Date
736	Dey, N., D. F. Socie, and K. J. Hsia	Static and cyclic fatigue failure at high temperature in ceramics containing grain boundary viscous phase, Part I: Experiments	Nov. 1993
737	Dey, N., D. F. Socie, and K. J. Hsia	Static and cyclic fatigue failure at high temperature in ceramics containing grain boundary viscous phase, Part II: Modeling—*Acta Metallurgica et Materialia*, **43**, 2163-2175 (1995)	Nov. 1993
738	Turner, J. A., and R. L. Weaver	Radiative transfer and multiple scattering of diffuse ultrasound in polycrystalline media—*Journal of the Acoustical Society of America* **96**, 3675–3681 (1994)	Nov. 1993
739	Qi, Q., and R. E. Johnson	Resin flows through a porous fiber collection in pultrusion processing	Dec. 1993
740	Weaver, R. L., W. Sachse, and K. Y. Kim	Transient elastic waves in a transversely isotropic plate—*Journal of Applied Mechanics*, in press (1996)	Dec. 1993
741	Zhang, Y., and R. L. Weaver	Scattering from a thin random fluid layer—*Journal of the Acoustical Society of America* **96**, 1899–1909 (1994)	Dec. 1993
742	Weaver, R. L., and W. Sachse	Diffusion of ultrasound in a glass bead slurry—*Journal of the Acoustical Society of America* **97**, 2094–2102 (1995)	Dec. 1993
743	Sundermeyer, J. N., and R. L. Weaver	On crack identification and characterization in a beam by nonlinear vibration analysis—*Journal of Sound and Vibration* **183**, 857–872 (1995)	Dec. 1993
744	Li, L., and N. R. Sottos	Predictions of static displacements in 1–3 piezocomposites—*Journal of Intelligent Materials Systems and Structures* **6**, 169–180 (1995)	Dec. 1993
745	Jones, S. W.	Chaotic advection and dispersion—*Physica D* **76**, 55–69 (1994)	Jan. 1994
746	Stewart, D. S., and J. Yao	Critical detonation shock curvature and failure dynamics: Developments in the theory of detonation shock dynamics—*Developments in Theoretical and Applied Mechanics* **17** (1994)	Feb. 1994
747	Mei, R., and R. J. Adrian	Effect of Reynolds-number-dependent turbulence structure on the dispersion of fluid and particles—*Journal of Fluids Engineering*, **117**, 402-409 (1995)	Feb. 1994
748	Liu, Z.-C., R. J. Adrian, and T. J. Hanratty	Reynolds-number similarity of orthogonal decomposition of the outer layer of turbulent wall flow—*Physics of Fluids* **6**, 2815–2819 (1994)	Feb. 1994
749	Barnhart, D. H., R. J. Adrian, and G. C. Papen	Phase-conjugate holographic system for high-resolution particle image velocimetry—*Applied Optics* **33**, 7159–7170 (1994)	Feb. 1994
750	Qi, Q., W. D. O'Brien Jr., and J. G. Harris	The propagation of ultrasonic waves through a bubbly liquid into tissue: A linear analysis—*IEEE Transactions on Ultrasonics, Ferroelectrics and Frequency Control* **42**, 28–36 (1995)	Mar. 1994
751	Mittal, R., and S. Balachandar	Direct numerical simulation of flow past elliptic cylinders—*Journal of Computational Mechanics*, in press (1996)	May 1994
752	Students in TAM 293–294	Thirty-first student symposium on engineering mechanics, J. W. Phillips, coordinator: Selected senior projects by D. N. Anderson, J. R. Dahlen, M. J. Danyluk, A. M. Dreyer, K. M. Durkin, J. J. Kriegsmann, J. T. McGonigle, and V. Tyagi	May 1994
753	Thoroddsen, S. T.	The failure of the Kolmogorov refined similarity hypothesis in fluid turbulence—*Physics of Fluids* **7**, 691–693 (1995)	May 1994
754	Turner, J. A., and R. L. Weaver	Time dependence of multiply scattered diffuse ultrasound in polycrystalline media—*Journal of the Acoustical Society of America* **97**, 2639–2644 (1995)	June 1994
755	Riahi, D. N.	Finite-amplitude thermal convection with spatially modulated boundary temperatures—*Proceedings of the Royal Society of London A* **449**, 459–478 (1995)	June 1994

No.	Authors	Title	Date
756	Riahi, D. N.	Renormalization group analysis for stratified turbulence—*International Journal of Mathematics and Mathematical Sciences*, in press (1996)	June 1994
757	Riahi, D. N.	Wave-packet convection in a porous layer with boundary imperfections—*Journal of Fluid Mechanics*, in press (1996)	June 1994
758	Jog, C. S., and R. B. Haber	Stability of finite element models for distributed-parameter optimization and topology design—*Computer Methods in Applied Mechanics and Engineering*, in press (1996).	July 1994
759	Qi, Q., and G. J. Brereton	Mechanisms of removal of micron-sized particles by high-frequency ultrasonic waves—*IEEE Transactions on Ultrasonics, Ferroelectrics and Frequency Control* **42**, 619–629 (1995)	July 1994
760	Shawki, T. G.	On shear flow localization with traction-controlled boundaries—*International Journal of Solids and Structures* **32**, 2751–2778 (1995)	July 1994
761	Balachandar, S., D. A. Yuen, and D. M. Reuteler	High Rayleigh number convection at infinite Prandtl number with temperature-dependent viscosity	July 1994
762	Phillips, J. W.	Arthur Newell Talbot—Proceedings of a conference to honor TAM's first department head and his family	Aug. 1994
763	Man., C. S., and D. E. Carlson	On the traction problem of dead loading in linear elasticity with initial stress—*Archive for Rational Mechanics and Analysis* **128**, 223–247 (1994)	Aug. 1994
764	Zhang, Y., and R. L. Weaver	Leaky Rayleigh wave scattering from elastic media with random microstructures	Aug. 1994
765	Cortese, T. A., and S. Balachandar	High-performance spectral simulation of turbulent flows in massively parallel machines with distributed memory—*International Journal of Supercomputer Applications* **9**, 185–202 (1995)	Aug. 1994
766	Balachandar, S.	Signature of the transition zone in the tomographic results extracted through the eigenfunctions of the two-point correlation—*Geophysical Research Letters* **22**, 1941–1944 (1995)	Sept. 1994
767	Piomelli, U.	Large-eddy simulation of turbulent flows	Sept. 1994
768	Harris, J. G., D. A. Rebinsky, and G. R. Wickham	An integrated model of scattering from an imperfect interface—*Journal of the Acoustical Society of America*, in press (1996)	Sept. 1994
769	Hsia, K. J., and Z.-Q. Xu	The mathematical framework and an approximate solution of surface crack propagation under hydraulic pressure loading—*International Journal of Fracture*, in press (1996)	Sept. 1994
770	Balachandar, S.	Two-point correlation and its eigen-decomposition for optimal characterization of mantle convection	Oct. 1994
771	Lufrano, J. M., and P. Sofronis	Numerical analysis of the interaction of solute hydrogen atoms with the stress field of a crack—*International Journal of Solids and Structures*, in press (1996)	Oct. 1994
772	Aref, H., and S. W. Jones	Motion of a solid body through ideal fluid	Oct. 1994
773	Stewart, D. S., T. D. Aslam, J. Yao, and J. B. Bdzil	Level-set techniques applied to unsteady detonation propagation—In "Modeling in Combustion Science," *Lecture Notes in Physics* (1995)	Oct. 1994
774	Mittal, R., and S. Balachandar	Effect of three-dimensionality on the lift and drag of circular and elliptic cylinders—*Physics of Fluids* **7**, 1841–1865 (1995)	Oct. 1994
775	Stewart, D. S., T. D. Aslam, and J. Yao	On the evolution of cellular detonation	Nov. 1994 *Revised* Jan. 1996

No.	Authors	Title	Date
776	Aref, H.	On the equilibrium and stability of a row of point vortices—*Journal of Fluid Mechanics* **290**, 167–181 (1995)	Nov. 1994
777	Cherukuri, H. P., T. G. Shawki, and M. El-Raheb	An accurate finite-difference scheme for elastic wave propagation in a circular disk—*Journal of the Acoustical Society of America,* in press (1996)	Nov. 1994
778	Li, L., and N. R. Sottos	Improving hydrostatic performance of 1–3 piezocomposites—*Journal of Applied Physics* **77**, 4595–4603 (1995)	Dec. 1994
779	Phillips, J. W., D. L. de Camara, M. D. Lockwood, and W. C. C. Grebner	Strength of silicone breast implants—*Plastic and Reconstructive Surgery* **97**, in press (1996)	Jan. 1995
780	Xin, Y.-B., K. J. Hsia, and D. A. Lange	Quantitative characterization of the fracture surface of silicon single crystals by confocal microscopy—*Journal of the American Ceramics Society* **78**, 3201-3208 (1995)	Jan. 1995
781	Yao, J., and D. S. Stewart	On the dynamics of multi-dimensional detonation—*Journal of Fluid Mechanics*, **309**, 225-275 (1996)	Jan. 1995
782	Riahi, D. N., and T. L. Sayre	Effect of rotation on the structure of a convecting mushy layer—*Acta Mechanica,* in press (1996)	Feb. 1995
783	Batchelor, G. K., and TAM faculty and students	A conversation with Professor George K. Batchelor	Feb. 1995
784	Sayre, T. L., and D. N. Riahi	Effect of rotation on flow instabilities during solidification of a binary alloy	Feb. 1995
785	Xin, Y.-B., and K. J. Hsia	A technique to generate straight surface cracks for studying the dislocation nucleation condition in brittle materials —*Acta Metallurgica et Materialia* **44**, 845-853 (1996).	Mar. 1995
786	Riahi, D. N.	Finite bandwidth, long wavelength convection with boundary imperfections: Near-resonant wavelength excitation	Mar. 1995
787	Turner, J. A., and R. L. Weaver	Average response of an infinite plate on a random foundation—*Journal of the Acoustical Society of America* **99**, in press (1996)	Mar. 1995
788	Weaver, R. L., and D. Sornette	The range of spectral correlations in pseudointegrable systems: GOE statistics in a rectangular membrane with a point scatterer—*Physical Review E*, **52**, 341 (1995)	April 1995
789	Students in TAM 293–294	Thirty-second student symposium on engineering mechanics, J. W. Phillips, coordinator: Selected senior projects by K. F. Anderson, M. B. Bishop, B. C. Case, S. R. McFarlin, J. M. Nowakowski, D. W. Peterson, C. V. Robertson, and C. E. Tsoukatos	April 1995
790	Figa, J., and C. J. Lawrence	Linear stability analysis of a gravity-driven Newtonian coating flow on a planar incline	May 1995
791	Figa, J., and C. J. Lawrence	Linear stability analysis of a gravity-driven viscosity-stratified Newtonian coating flow on a planar incline	May 1995
792	Cherukuri, H. P., and T. G. Shawki	On shear band nucleation and the finite propagation speed of thermal disturbances—*International Journal of Solids and Structures,* in press (1996)	May 1995
793	Harris, J. G.	Modeling scanned acoustic imaging of defects at solid interfaces—Chapter in *IMA Workshop on Inverse Problems in Wave Propagation,* Springer-Verlag, to appear (1996)	May 1995
794	Sottos, N. R., J. M. Ockers, and M. J. Swindeman	Thermoelastic properties of plain weave composites for multilayer circuit board applications	May 1995

List of Recent TAM Reports (cont'd)

No.	Authors	Title	Date
795	Aref, H., and M. A. Stremler	On the motion of three point vortices in a periodic strip—*Journal of Fluid Mechanics*, in press (1996).	June 1995
796	Barenblatt, G. I., and N. Goldenfeld	Does fully-developed turbulence exist? Reynolds number independence versus asymptotic covariance—*Physics of Fluids* **7**, 3078–3082 (1995)	June 1995
797	Aslam, T. D., J. B. Bdzil, and D. S. Stewart	Level set methods applied to modeling detonation shock dynamics—*Journal of Computational Physics*, in press (1996)	June 1995
798	Nimmagadda, P. B. R., and P. Sofronis	The effect of interface slip and diffusion on the creep strength of fiber and particulate composite materials—*Mechanics of Materials*, in press (1996)	July 1995
799	Hsia, K. J., T.-L. Zhang, and D. F. Socie	Effect of crack surface morphology on the fracture behavior under mixed mode loading —*ASTM Special Technical Publications*, STP 1296, in press (1996)	July 1995
800	Adrian, R. J.	Stochastic estimation of the structure of turbulent fields	Aug. 1995
801	Riahi, D. N.	Perturbation analysis and modeling for stratified turbulence	Aug. 1995
802	Thoroddsen, S. T.	Conditional sampling of dissipation in high Reynolds number turbulence —*Physics of Fluids*, in press (1996)	Aug. 1995
803	Riahi, D. N.	On the structure of an unsteady convecting mushy layer	Aug. 1995
804	Meleshko, V. V.	Equilibrium of an elastic rectangle: The Mathieu–Inglis–Pickett solution revisited—*Journal of Elasticity* **40**, 207-238 (1995)	Aug. 1995
805	Jonnalagadda, K., G. E. Kline, and N. R. Sottos	Local displacements and load transfer in shape memory alloy composites	Aug. 1995
806	Nimmagadda, P. B. R., and P. Sofronis	On the calculation of the matrix–reinforcement interface diffusion coefficient in composite materials at high temperatures—*Acta Metallurgica et Materialia*, in press (1996)	Aug. 1995
807	Carlson, D. E., and D. A. Tortorelli	On hyperelasticity with internal constraints—*Journal of Elasticity*, in press (1996)	Aug. 1995
808	Sayre, T. L., and D. N. Riahi	Oscillatory instabilities of the liquid and mushy layers during solidification of alloys under rotational constraint—*Acta Mechanica*, in press (1996)	Sept. 1995
809	Xin, Y.-B., and K. J. Hsia	Simulation of the brittle-ductile transition in silicon single crystals using dislocation mechanics	Oct. 1995
810	Ulysse, P., and R. E. Johnson	A plane-strain upper-bound analysis of unsymmetrical single-hole and multi-hole extrusion processes	Oct. 1995
811	Fried, E.	Continua described by a microstructural field—*Zeitschrift für angewandte Mathematik und Physik*, in press (1996)	Nov. 1995
812	Mittal, R., and S. Balachandar	Autogeneration of three-dimensional vortical structures in the near wake of a circular cylinder	Nov. 1995
813	Segev, R., E. Fried, and G. de Botton	Force theory for multiphase bodies—*Journal of Geometry and Physics*, in press (1996)	Dec. 1995
814	Weaver, R. L.	The effect of an undamped finite-degree-of-freedom "fuzzy" substructure: Numerical solutions and theoretical discussion	Jan. 1996
815	Haber, R. B., C. S. Jog, and M. P. Bensøe	A new approach to variable-topology shape design using a constraint on perimeter—*Structural Optimization* **11**, 1-12 (1996)	Feb. 1996
816	Xu, Z.-Q., and K. J. Hsia	A numerical solution of a surface crack under cyclic hydraulic pressure loading	Mar. 1996
817	Adrian, R. J.	Bibliography of particle velocimetry using imaging methods: 1917–1995	Mar. 1996